

# Model-Agnostic Explainability for Visual Search

Mark Hamilton<sup>1,2</sup> Scott Lundberg<sup>2</sup> Lei Zhang<sup>2</sup> Stephanie Fu<sup>1</sup> William T. Freeman<sup>1,3</sup>

## Abstract

What makes two images similar? We propose new approaches to generate model-agnostic explanations for image similarity, search, and retrieval. In particular, we extend Class Activation Maps (CAMs), Additive Shapley Explanations (SHAP), and Locally Interpretable Model-Agnostic Explanations (LIME) to the domain of image retrieval and search. These approaches enable black and grey-box model introspection and can help diagnose errors and understand the rationale behind a model’s similarity judgments. Furthermore, we extend these approaches to extract a full pairwise correspondence between the query and retrieved image pixels, an approach we call “joint interpretations”. Formally, we show joint search interpretations arise from projecting Harsanyi dividends, and that this approach generalizes Shapley Values and The Shapley-Taylor indices. We introduce a fast kernel-based method for estimating Shapley-Taylor indices and empirically show that these game-theoretic measures yield more consistent explanations for image similarity architectures.

## 1. Introduction

Text, image, and audio search engines are ubiquitous in our everyday life and help us navigate a world of information orders of magnitude larger than any one human could read in their lifetime. Search engines are growing increasingly complicated and can utilize billion-parameter models (Nayak, 2019). Despite search’s foundational importance, there is a lack of principled techniques to understand the rationale behind a search engine’s matches and responses. At its core, these systems face the same challenges that classifiers and regressors face: richer model spaces can improve performance but yield un-interpretable models. For high-risk domains like medicine, incorrect search results could result in serious consequences. In other domains, bias in a search engine can disproportionately hide certain voices and have far-reaching systemic consequences.

To help solve this challenge, we present a unified framework for extending model interpretability to search engines, recommendation systems, and retrieval systems. With these

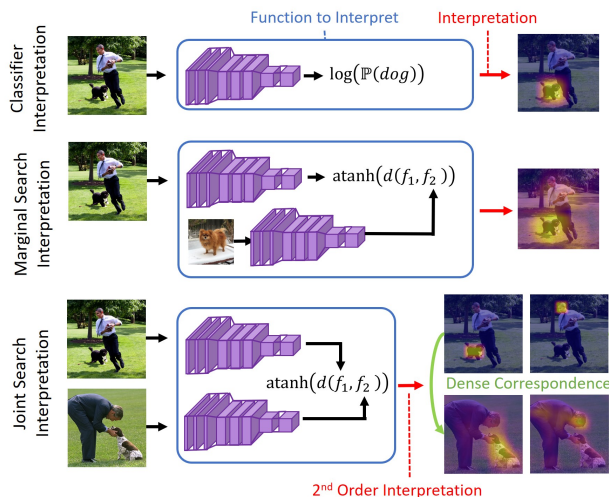


Figure 1. Architectures for search engine interpretability. Top: Standard classifier interpretation that highlights pixels that contribute to the prediction. Middle: Our marginal search interpretation architecture modifies the classifier interpretation architecture to highlight pixels that contribute to the similarity between images. Bottom: “Joint” search interpretation extracts a full pairwise correspondence between objects in the query and retrieved image, all while treating the search engine as a black box.

tools, practitioners can gain insight into the rationales behind their algorithm’s matches *without* knowledge of an algorithm’s internal construction. We explore this topic through the lens of visual search, but note that these techniques could also apply to text, tabular, or audio systems. This work identifies two distinct ways to interpret search engines: “Marginal Interpretations” highlight the most important pixels in the match and “Joint Interpretations” extract a full correspondence between query and retrieved image pixels. To extract marginal interpretations we introduce a generic transformation, as shown in Figure 1, to transform search engines and retrieval systems into “classifiers” that can be interpreted with existing classifier interpretation methods. To extract joint interpretations, we present new bilinear generalizations of Class Activation Maps (Zhou et al., 2016), LIME (Ribeiro et al., 2016), and SHAP (Lundberg & Lee, 2017). These joint interpretations are new to the literature and give practitioners tools to understand search engines with much greater nuance and detail. Formally, we axiomatically characterize joint interpretations and show that projecting Harsanyi Dividends (Harsanyi, 1963) pro-

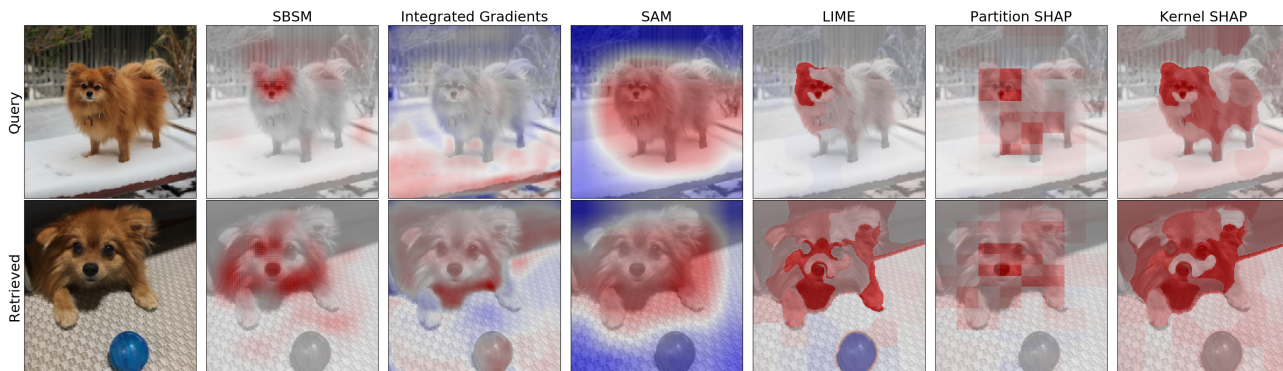


Figure 2. Comparison of marginal search interpretation methods. All methods identify pixels that most contribute to the image’s similarity. One exception is Integrated Gradients which struggles, in part because well trained classifiers are invariant to minor pixel changes and which results in uninformative gradients.

vides a unique solution to this characterization. This not only extends a correspondence between model explainability and cooperative game theory, but also yields better empirical results on a search engine evaluated on the PASCAL VOC dataset (Everingham et al., 2010). In summary:

- We introduce and evaluate new, *model-agnostic*, methods for interpreting search engines and recommendation systems.
- We extend existing approaches to extract full pairwise correspondences between item characteristics from similarity judgments.
- We relate search engine interpretability to the theory of Harsanyi Dividends, and show that this provides a simple way to calculate optimal credit-assignment schemes for more complex settings like search.

## 2. Background

This work focuses on search, retrieval, and recommendation architectures. Often, these systems use similarity between objects or learned features (Bengio et al., 2013) to rank, retrieve, or suggest content (Bing, 2017; Su & Khoshgoftaar, 2009). More formally, we refer to systems that leverage a distance, relevance, or similarity functions of the form:  $d : \mathcal{X} \times \mathcal{Y} \rightarrow \mathbb{R}$  to quantify the relationship between items from sets  $\mathcal{X}$  and  $\mathcal{Y}$ . In search and retrieval,  $\mathcal{X}$  represents the space of search queries and  $\mathcal{Y}$  represents the space of results, the function  $d$  assigns a relevance to each query result pair. Finding the most relevant results for a query  $x \in \mathcal{X}$  takes the form:

$$\arg \max_{y \in \mathcal{Y}} d(x, y)$$

Specializing this notion yields a variety of different kinds of ML systems. If  $\mathcal{X} = \mathcal{Y} = \text{Range}(\mathcal{N}(\cdot))$  where  $\mathcal{N}$  is an

image featurization network such as ResNet50 (He et al., 2016), the formalism yields a visual search engine or “reverse image search”. Though this work focuses on visual search, we note that if  $\mathcal{X}$  is the space of character sequences and  $\mathcal{Y}$  is the space of webpages, this represents web search. If  $\mathcal{X}$  are users and  $\mathcal{Y}$  are the space of items, such as songs or news articles, the formalism represents a recommendation problem. In this work we aim to extract meaningful “interpretations” or “explanations” of the function  $d$ .

### 2.1. Model Interpretability

The Bias-Variance trade-off (Kohavi et al., 1996) affects all machine learning systems and governs the relationship between a model’s expressiveness and generalization ability. In data-rich scenarios, generalization error is dominated by a model’s bias and increasing the size of the model class can improve performance. However, increasing model complexity can severely degrade its “interpretability”. Larger model classes have more parameters to interpret and these parameters can lose their connection to physically meaningful quantities. This is a challenge not just for classification and regression systems, but for search and recommendation architectures as well. For example, the best performing competitors on the Netflix prize dataset (Bennett et al., 2007) involve significantly more complex models than earlier baselines (Rendle et al., 2019). Famously, the Netflix grand prize winner, the “BellKor” algorithm (Koren, 2009), boosts and ensembles several different underlying methods making it difficult to interpret the model by inspecting its parameters.

To tackle these challenges, some works introduce model classes that are naturally interpretable (Nori et al., 2019; Hastie & Tibshirani, 1990). Alternatively, to other works have proposed *model-agnostic* methods to “explain” the predictions of classifiers and regressors. Many of these approaches try to model and explain the “local” structure around a specific prediction. For example, the black-box

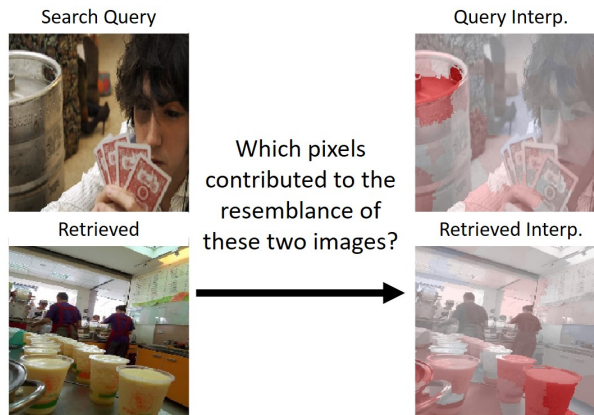


Figure 3. A pair of incorrectly matched images and their corresponding marginal interpretations from Kernel SHAP which highlight important pixels in red. This visualization shows that the search engine noticed similarity between the keg and the cup, due to the geometry of these objects.

interpretability method LIME samples the model’s behavior around a neighborhood of a prediction and distills this behavior with a simpler interpretable model like a distance-weighted, regularized, linear model. Other approaches like DeepLift and Layer-wise relevance propagation project signal from a deep network prediction backwards through the network structure. Class Activation Maps (CAMs) project the predicted class of a deep convolutional network onto the penultimate features to create a low resolution heatmap of class-specific network attention. This yields robust interpretations with only a single network evaluation, and has applications in weakly supervised semantic and instance segmentation (Ahn et al., 2019; Wang et al., 2020). Finally, Additive Shapley Explanations (SHAP), uses the notion of optimal credit assignment through Shapley Values (Shapley, 1951) to weight each feature’s importance in a prediction. Importantly, (Lundberg & Lee, 2017) showed that LIME, DeepLift (Shrikumar et al., 2017), Layer-Wise Relevance Propagation (Bach et al., 2015), and Integrated Gradients (Sundararajan et al., 2017) are all implicitly approximating the Shapley Value and thus provided a unified understanding of these methods. We extend this connection in our work.

### 3. Marginal Search Interpretability

Though there is a considerable amount of literature on classifier interpretability, black-box search engine interpretability has only recently been investigated. We build on the rich classifier interpretability literature to present a general transformation that allows one to extend model agnostic explanations to a broader class of systems such as search engines, recommendation systems, and content-based retrieval algorithms. This approach extracts the features, words, or

superpixels of the data that contribute the most to the overall similarity judgement. More formally, given a similarity function  $d : \mathcal{X} \times \mathcal{Y} \rightarrow \mathbb{R}$  and elements  $x \in \mathcal{X}$  and  $y \in \mathcal{Y}$  we form the following pair of functions:

$$f_y(x) : \mathcal{X} \rightarrow \mathbb{R} := f_{link}(d(x, y)) \quad (1)$$

$$f_x(y) : \mathcal{Y} \rightarrow \mathbb{R} := f_{link}(d(x, y)) \quad (2)$$

Where  $f_{link}$  is a function to transform the output of  $d$  so that explanations have more natural and additive units resembling log-odds for classification (Lundberg & Lee, 2017; Nelder & Wedderburn, 1972). For the commonly used cosine similarity between features shown in Figure 1, we use  $\text{atanh} : [-1, 1] \rightarrow \mathbb{R}$ . By using these functions with existing classifier interpretability techniques like LIME, SHAP, DeepLift, and Layer-wise relevance propagation we can compute the most important features, superpixels, or words in both the query,  $x$  and retrieved data,  $y$ , respectively. We refer to this approach as “marginal” search interpretability as it finds important substructure within  $x$  and  $y$  but does not generate a “correspondence” between the structures of  $x$  and  $y$ . In Section 4.4 we discuss this connection in greater detail.

Figure 1 middle row demonstrates this approach applied to a simple deep visual search architecture where a deep network featurizes both query and retrieved images before comparing their similarity. Transforming the search query via partial function application and using different link function ( $f_{link} = \text{atanh}$ ) enables direct use of existing model-interpretability approaches. We compare these approaches visually in Figure 2.

In addition to extending black-box interpretation methods to search we also extend the white-box convolution network interpretation approach, CAM, to search. We refer to this approach as “Search Activation Maps (SAM)”. CAM and SAM are both apply to convolutional networks with a penultimate global average pooling layer. Despite this limitation, CAM is widely used because it only requires a single forward pass of the network and is fully differentiable. Differentiability allows CAM regularization and manipulation in more complex vision architectures (Wang et al., 2020). To generalize CAM to search and recommendation architectures, let  $f_{hwc}$  represent the layer of activations of the query image before the global average pooling layer with spatial height  $h$ , width  $w$ , and feature size  $c$ . Let the function  $\text{norm}_c$  represent normalization with respect to the channel dimension  $c$ . Let  $g_c$  represent the average pooled activations of the retrieved image. Contracting  $f$  and  $g$  along the “feature” dimension  $c$  yields an attention map  $a_{hw}$  over the query image. In Einstein notation (Einstein, 1923):

$$a_{hw} := \text{norm}_c(f_{hwc}) \text{norm}_c(g^c) \quad (3)$$



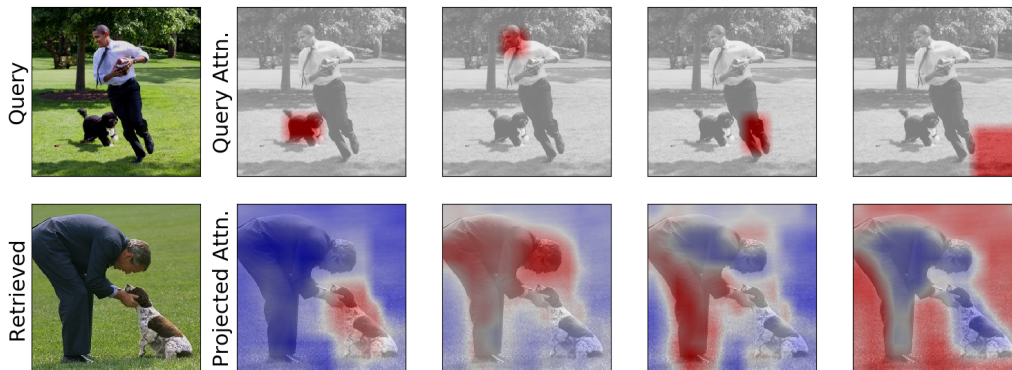


Figure 4. Visualization of how regions of two similar images can be put in correspondence through the joint search interpretability method SAM. This correspondence also allows us to transfer labels or attention between similar images in a principled way.

Like CAM, SAM can be overlaid on query image pixels to visualize the regions that most contribute to the similarity. Additionally, one can switch the query and target images in the above formulation to visualize attention over the retrieved image pixels.

Visualizing why pairs of images are considered similar can help model users and builders understand their retrieval systems. For example, Figure 3 demonstrates how this approach can identify why a particular image search system erroneously matched a pair of irrelevant images. This is analogous to how classifier interpretation approaches allow model designers to diagnose errors (Ribeiro et al., 2016).

## 4. Joint Search Interpretability

Visualizing the pixels that most “explain” the similarity judgement provides a simple way to inspect where a black-box search engine is “attending to”. However, this visualization is only part of the story. Image pairs can be similar for many different reasons, and a good explanation should clearly delineate these independent reasons. For example, consider the pair of images in the bottom left of Figure 1. These images show two similar scenes of people playing with dogs with several similar objects, but in different arrangements. We seek not just a heatmap highlighting similar aspects, but a data-structure which tells us about how parts of the query image *correspond* to parts of a target image and vice-versa. In this section we will present generalizations of CAM, LIME, and SHAP to this richer interpretation setting.

### 4.1. Joint Search Activation Maps (SAM)

We begin with generalizing CAM to the joint setting. By modifying the tensor contraction used in marginal SAM, we can compute a tensor which represents the affinities between regions of the query and retrieved images. More formally, let  $f_{hwc}$ , represent the layer of activations of the

query image before the global average pooling layer of a trained convolutional network. This tensor has spatial height  $h$ , width  $w$ , and feature size  $c$ . Let  $g^{ijc}$  represent the corresponding tensor of activations for the retrieved images with spatial dimensions  $i$ , and  $j$ . Contracting these tensors across  $c$  yields:

$$a_{hw}^{ij} := \text{norm}_c(h_{hwc}) \text{norm}_c(g^{ijc}) \quad (4)$$

Which is a fourth rank tensor whose values are cosine distances between each combination of features in the query and retrieved image. This tensor not only captures the fine-grained correspondence between query and retrieved images, but also has an operational interpretation as a transport mapping which can project “attention” from the query to the retrieved image and vice-versa. We elaborate on this connection in Section 4.4.

### 4.2. Joint Search LIME

Next, we generalize LIME to provide joint search interpretations. In the classifier formulation of LIME, one fits a locally-weighted and regularized linear approximation to the neighborhood of a particular model’s prediction. For image classifiers, one forms thus “neighborhood” by decomposing the input image into superpixels (Achanta et al., 2010) and perturbing the image by replacing random superpixels with a background color. This process is called “toggling” the superpixels, and the boolean states of these superpixels are used to form the features of a linear regression dataset. The “targets” are the log probabilities given to the perturbed images by the image classifier under examination. Fitting a locally weighted and regularized linear model to this dataset captures the impact of each superpixel on the prediction. In particular, the fit model is of the form:

$$y \sim a_0 + \sum_q a_q s_q \quad (5)$$

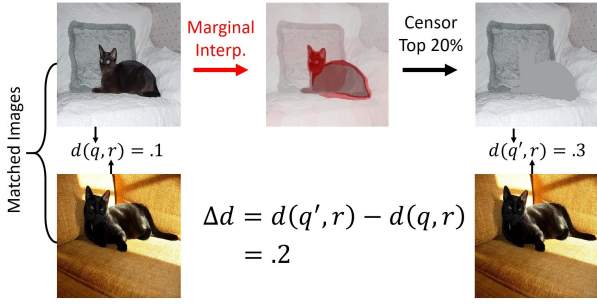


Figure 5. Marginal interpretation evaluation strategy. A good method should highlight pixels in the query image (top left and middle) that, when censored (top right), have the largest possible impact on the similarity.

Where  $s_q = 1$  when a superpixel  $q$  is toggled “on” and the learned weights  $a_q$  represent the impact of each superpixel. We point readers to the original work (Ribeiro et al., 2016) for a more detailed description of the approach. To generalize LIME to the domain of joint search interpretability we instead consider locally approximating the search engine with a regularized *bi-linear* approximation to capture cross image interactions. More specifically, we decompose both query and retrieved images into superpixels and form a dataset by toggling superpixels in both images simultaneously. We then map these “perturbed” pairs through similarity function  $d$  and the link function  $f_{link}$ . Finally, we fit a bi-linear model of the form:

$$y \sim a_0 + \sum_q a_q s_q + \sum_r a_r s_r + \sum_{q,r} a_{qr} s_q s_r \quad (6)$$

Where  $s_q$  are the indicator variables that a superpixel,  $q$ , in the query image is toggled on, and likewise  $s_r$  indicates the presence of superpixel  $r$  in the retrieved image. The model parameters:  $a_0$ ,  $a_q$ ,  $a_r$ , and  $a_{qr}$  are the learned constant, query-linear, retrieved-linear, and bi-linear terms, respectively. As in the original implementation of LIME, one can include a local weighting when fitting the bi-linear model to increase the influence of less-perturbed pairs of images and a L1 penalty to increase the sparsity of solutions.

### 4.3. Joint Search SHAP

Additive Shapley Explanations supply a principled and axiomatic framework for classifier interpretation and unify several existing approaches. This work looks to extend this framework to the richer functional forms and interpretations needed for search and recommendation systems. SHAP explains predictions by weighting features according to how much “credit” each receives for the prediction in an optimal credit assignment framework. More formally, a “coalition game” is a set  $N$  of  $n$  players and a function  $v : 2^N \rightarrow \mathbb{R}$  where  $v(\emptyset) = 0$ . In cooperative game theory, this function

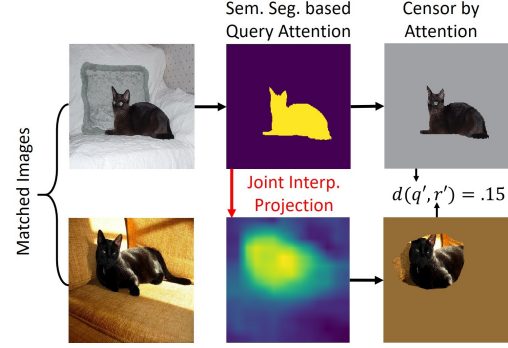


Figure 6. Joint interpretation evaluation strategy. A good method should project query image attention (top left and middle) to corresponding structure in the retrieved image (bottom left and middle). When censoring all but this shared structure (right column) the search engine should view these images as similar.

$v$  represents the expected payoff for a given cooperating coalition of players. Shapley Value Theory shows that the unique, fair credit assignment to each player,  $\phi_v(i \in N)$ , can be calculated as:

$$\phi_v(i) := \sum_{T \subseteq N \setminus \{i\}} \frac{|T|!(n - |T| - 1)!}{n!} (v(T \cup \{i\}) - v(T)) \quad (7)$$

This equation captures the average increase in value that a player  $i$  brings to a coalition  $T$  by weighting each increase,  $v(T \cup \{i\}) - v(T)$ , by the number of ways this event could have happened during the formation of the “grand coalition”  $N$ . We note that this assignment,  $\phi_v$ , is the only one that satisfies four reasonable properties: Symmetry under player re-labeling, no credit assignment to “dummy” players, linearity, and “efficiency” which states that Shapley values should sum to  $v(N)$  (Young, 1985). To connect this work to model interpretability, one can identify the “features” used in model as the “players” and interpret the characteristic function,  $v(T)$ , as the expected prediction of the model with features corresponding to  $N \setminus T$  replaced by values from a “background” distribution. In our experiments we use a blank image.

To guide our generalization of SHAP we note that both SAM and LIME generalize to joint interpretation methods by replacing linear forms with multi-linear forms to capture interactions between the query and retrieved images. Following this pattern, we seek higher order generalizations of the Shapley Value. In particular (Harsanyi, 1963) show that the Shapley Values arise from distributing “Harsanyi dividends” associated with every coalition of players, evenly across members of the coalition. More specifically, the Harsanyi Dividend for a coalition  $S$  is defined as:

$$d_v(S) := \begin{cases} v(S) & \text{if } |S| = 1 \\ v(S) - \sum_{T \subset S} d_v(T) & \text{if } |S| > 1 \end{cases} \quad (8)$$

These dividends, also known as Möbius coefficients (Grabisch et al., 2016), provide a detailed view of the function’s behavior at every coalition. In this work we generalize the notion of sharing these dividends between individuals to sharing these dividends between sub-coalitions. This insight provides natural motivation for a recent Generalization of Shapley Values called the Shapley-Taylor Indices (Sundararajan et al., 2020). More specifically, (Sundararajan et al., 2020) define a generalization of the Shapley Values to coalitions of a size  $k$  using the discrete derivative operator, which leads to their namesake connection with Taylor series expansions. However, we show that in the language of Harsanyi Dividends the connection between the Shapley Values and the Shapley-Taylor index is much more apparent. Through the lens of sharing dividends, we arrive at a new formula for the Shapley-Taylor values for coalitions  $|S| = k$ :

$$\phi_v^k(S) = \sum_{T: S \subset T} \frac{d_v(T)}{\binom{|T|}{|S|}} \quad (9)$$

In this light, one can see that Shapley-Taylor values simply divide up the high order Harsanyi Dividends evenly among all lower-order terms. This reproduces the Shapley Values when  $k = 1$ . When  $k = 2$  it assigns credit to each individual  $|S| = 1$  and pair of individuals  $|S| = 2$ . This insight not only allows for deriving the Shapley Values and the Shapley-Taylor indices, but also allows for the creation of new optimal credit assignment weights for more complex problems. In our motivating example of interpreting visual search engines, we keep terms associated with each superpixel, and cross-image pairs of superpixels (first superpixel is in the query image, and the second superpixel is in the retrieved image). We divide all other dividends and distribute them their smaller coalitions. This “cross-linear” optimal credit assignment has the same binary terms as the Shapley-Taylor indices, but different unary terms due to the splitting of intra-image terms among the individual superpixels. Put another way, Harsanyi dividend sharing allows one to create “jagged” generalizations of the Shapley-Taylor indices that can yield optimal credit assignments on more complex collections of coalitions.

Though the Harsanyi Dividends and Shapley-Taylor indices provide a robust way to allocate credit, they are difficult to compute. The authors of the Shapley-Taylor indices provide a sampling-based approximation, but this approach requires estimating each interaction term with a separate sampling procedure, which scales poorly as dimensionality increases. To make this approach more tractable for large scale datasets we draw a parallel the unification of LIME with Shapley Values through a specific weighting kernel. In particular we introduce a kernel for second order Shapley-Taylor indices:

$$k(N, S) = \frac{|N| - 1}{\binom{|N|}{|S|} \binom{|S|}{2} (|N| - |S|)} \quad (10)$$

Using this kernel, one can instead sample random coalitions, evaluate  $v$ , and aggregate the information into a bilinear model. This allows one to approximate all Shapley-Taylor indices of  $k = 2$  with a single sampling procedure, and converges much faster for high dimensional problems and we report convergence rates in Section B of the Supplement. This also allows us to view joint search LIME as a Shapley-Taylor index approximator much like regular LIME is to the Shapley Values.

#### 4.4. Connection to Attention Transport

Beyond measuring of the interaction strength between regions in the query and retrieved image, joint explanations also have an operational interpretation as a method of attention transportation between images. For example in Equation 4 which characterizes Joint SAM the co-variant and contra-variant positions of the spatial indices indicate that the tensor,  $a_{hw}^{ij}$ , also encodes a mapping. More specifically, let  $q^{hw}$  denote an attention map over the query image, we form a corresponding attention map on the retrieved image using the tensor contraction:  $r^{ij} := a_{hw}^{ij} q^{hw}$ . Figure 4 demonstrates how projecting different localized attention maps can visualize detailed information about how specific regions of the query image correspond to regions of the target image.

By normalizing the joint interpretation tensor, the connection to transport theory becomes even more explicit. More specifically, we can view the normalized attention weights as a joint distribution over pairs of regions. The marginals of this distribution are precisely the marginal search interpretations. In summary, because a joint distribution encodes a transport plan between its marginals (Dobrushin, 1970), a joint interpretation acts as a transport plan between the marginal interpretations.

For LIME and Kernel SHAP, these transport strategies occur in the superpixel space rather than the image region space. In particular, one can use the interaction terms as a linear map to transfer attention from query to retrieved image superpixels. One can then project the weights onto the pixels by coloring each superpixel with its attention.

## 5. Experimental Evaluation

Evaluating the faithfulness of an interpretability method requires careful experimental design. Interpretations that “look good” to a human might not be faithful to the underlying model which could model the task poorly. We aim to evaluate how well our proposed joint and marginal interpretation approaches capture the structure of the underlying



search engine independent of how the model performs semantically. To this end we expand the “interpret-and-censor” evaluation strategy of (Lundberg & Lee, 2017). This approach first interprets a prediction, then censors the most important features, and finally re-evaluates the classifier. If the interpretation method works well, this should yield a large change in the prediction. The most important part of this method is that it directly measures faithfulness to the underlying classifier and does not conflate this with the performance of the classifier on the task.

### 5.1. Marginal Search Interpretation

We first generalize the interpret-and-censor evaluation to marginal search interpretation methods. Intuitively speaking, a good marginal search interpretation should highlight the “most important” pixels that contribute to the similarity of the two images. Censoring these important pixels by filling them with a mean-color background should dramatically reduce the similarity between these two images. The magnitude of the change in the similarity,  $\Delta d$ , between uncensored and censored image pairs is a direct measurement of the interpretability method’s quality and is a direct analogue of the interpret-and-censor strategy of (Lundberg & Lee, 2017). Figure 5 shows a diagram and example of our proposed strategy. We use each marginal interpretation strategy to extract an attention map over the query image pixels. Finally, we censor the top 20% of important pixels in the query and re-evaluate the engine’s similarity computation and record the change in distance,  $\Delta d$ . The marginal columns of Table 1 show the results of this experiment, and compares computation times across marginal methods, we find that SAM is the k, fastest method, but that PartitionSHAP provides the best quality interpretations and significantly outperforms the current best visual search approach SBSM (Dong et al.). The dominance of Partition SHAP suggests that the formal basis for SHAP also yields higher-fidelity interpretation methods. We describe our models, data, and implementation details in Section 5.3

### 5.2. Joint Search Interpretation

We also extend the interpret-and-censor evaluation strategy to joint interpretations by evaluating an interpretation’s ability to project attention maps. We generate different query attention maps using Pascal VOC’s ground truth semantic segmentation labels. Intuitively speaking, a good joint interpretation should find the region of the retrieved image that most closely matches a selected region of the query image. Censoring all but this region, as shown in Figure 6, should yield similar images according to the search engine. More specifically, first we censor the query image to a randomly chosen semantic segmentation class. Second, we use the chosen class’ segmentation mask as a query attention map attention and project this attention to the retrieved image

using the joint interpretation method. Third we then censor all but the top  $p$  pixels of the retrieved image where,  $p$  is the size of corresponding semantic segmentation mask in the retrieved image. Finally, we measure the similarity between the censored images. A faithful interpretation approach should yield a similar (small  $d$ ) image pair after censoring.

In addition to measuring faithfulness of the representation method we also measure how well the approach performs semantic segmentation label propagation. To measure this, we treat the projected attention as a binary semantic segmentation prediction and compare with the known ground truth segmentation labels. The mean intersection over union (mIoU) of this segmentation prediction provides a second measurement of interpretation quality more focused on a particular downstream task like label propagation. However, we caution that this is not a direct measurement of interpretation faithfulness, but we feel this provides a complementary view that can help creation of better label propagation systems. The joint columns of Table 1 show the results of these experiments over several interpretation methods that we have generalized to the joint domain. We find that SAM is by far the fastest but Kernel SHAP significantly outperforms all methods in terms of faithfulness to the underlying search engine. We describe our models, data, and implementation details in Section 5.3

We note that because this is the first work to identify these joint interpretations, there are no existing approaches in the literature to compare against in the joint domain. To compare against a reasonable literature-derived benchmark, we have additionally generalized the SBSM method to the joint setting and detail this construction in the Supplement.

### 5.3. Implementation Details

Our evaluation experiments use visual search engine built from a pre-trained “backbone” network that featurizes images and compares their similarity using cosine distance. We report results for engines using ResNet50 (He et al., 2016), VGG11 (Simonyan & Zisserman, 2014), and DenseNet121 (Huang et al., 2017), as backbone networks. We use 200 random query images from the Pascal VOC validation set and their closest pairs in the VOC training set. Additionally, we restrict retrieved images so that the query and retrieved images both contain the same class objects and have objects that take up more than 5% of the image (Hamilton et al., 2020). We include these image pairs and evaluation code in the supplement. Experiments use PyTorch (Paszke et al., 2019) v1.7 pre-trained models, on an Ubuntu 16.04 Azure NV24 Virtual Machine with Python 3.6.

Table 1. Comparison of speed and performance of marginal and joint search interpretation methods across three different search engines.  $\Delta d$  (higher is better) represents the change in similarity when censoring the top 20% of pixels in the marginal interpretation as shown in Figure 5.  $d$  (lower is better) is the similarity between attention-censored images as shown in Figure 6. mIoU (higher is better) represents the performance on a binary semantic segmentation label propagation task as described in Section 5.2.

| SEARCH BACKBONE | METHOD               | MARGINAL                           |                                    | JOINT                              |                                    | mIoU        |
|-----------------|----------------------|------------------------------------|------------------------------------|------------------------------------|------------------------------------|-------------|
|                 |                      | TIME (S)                           | $\Delta d$                         | TIME (S)                           | $d$                                |             |
| RESNET50        | SBSM                 | 19.5 $\pm$ 0.0                     | 0.1 $\pm$ 0.003                    | 87.4 $\pm$ 0.01                    | 0.32 $\pm$ 0.005                   | 0.52        |
|                 | SAM                  | <b>0.09 <math>\pm</math> 0.001</b> | 0.07 $\pm$ 0.003                   | <b>0.03 <math>\pm</math> 0.0</b>   | 0.27 $\pm$ 0.003                   | <b>0.65</b> |
|                 | LIME                 | 32.6 $\pm$ 0.02                    | 0.11 $\pm$ 0.004                   | 120.9 $\pm$ 0.06                   | 0.26 $\pm$ 0.004                   | 0.62        |
|                 | INTEGRATED GRADIENTS | 3.4 $\pm$ 0.0                      | 0.1 $\pm$ 0.004                    | -                                  | -                                  | -           |
|                 | KERNEL SHAP          | 44.4 $\pm$ 0.1                     | 0.11 $\pm$ 0.004                   | 129.4 $\pm$ 0.87                   | <b>0.25 <math>\pm</math> 0.005</b> | <b>0.65</b> |
|                 | PARTITION SHAP       | 45.0 $\pm$ 0.01                    | <b>0.15 <math>\pm</math> 0.004</b> | -                                  | -                                  | -           |
| VGG11           | SBSM                 | 16.3 $\pm$ 0.01                    | 0.12 $\pm$ 0.005                   | 68.7 $\pm$ 0.02                    | 0.41 $\pm$ 0.007                   | 0.53        |
|                 | SAM                  | <b>0.07 <math>\pm</math> 0.003</b> | 0.1 $\pm$ 0.005                    | <b>0.05 <math>\pm</math> 0.001</b> | <b>0.31 <math>\pm</math> 0.003</b> | <b>0.72</b> |
|                 | LIME                 | 29.8 $\pm$ 0.02                    | 0.12 $\pm$ 0.005                   | 109.0 $\pm$ 0.04                   | 0.32 $\pm$ 0.005                   | 0.63        |
|                 | INTEGRATED GRADIENTS | 3.1 $\pm$ 0.01                     | 0.08 $\pm$ 0.005                   | -                                  | -                                  | -           |
|                 | KERNEL SHAP          | 41.4 $\pm$ 0.07                    | 0.12 $\pm$ 0.005                   | 115.5 $\pm$ 0.71                   | <b>0.31 <math>\pm</math> 0.006</b> | 0.67        |
|                 | PARTITION SHAP       | 41.5 $\pm$ 0.03                    | <b>0.16 <math>\pm</math> 0.006</b> | -                                  | -                                  | -           |
| DENSENET121     | SBSM                 | 21.4 $\pm$ 0.01                    | 0.16 $\pm$ 0.006                   | 88.5 $\pm$ 0.01                    | 0.6 $\pm$ 0.008                    | 0.54        |
|                 | SAM                  | <b>0.17 <math>\pm</math> 0.004</b> | 0.14 $\pm$ 0.006                   | <b>0.12 <math>\pm</math> 0.001</b> | 0.52 $\pm$ 0.005                   | 0.63        |
|                 | LIME                 | 34.4 $\pm$ 0.02                    | 0.18 $\pm$ 0.006                   | 130.5 $\pm$ 0.06                   | 0.5 $\pm$ 0.006                    | 0.62        |
|                 | INTEGRATED GRADIENTS | 3.6 $\pm$ 0.0                      | 0.14 $\pm$ 0.007                   | -                                  | -                                  | -           |
|                 | KERNEL SHAP          | 46.2 $\pm$ 0.06                    | 0.19 $\pm$ 0.007                   | 130.5 $\pm$ 1.03                   | <b>0.49 <math>\pm</math> 0.008</b> | <b>0.65</b> |
|                 | PARTITION SHAP       | 47.6 $\pm$ 0.02                    | <b>0.24 <math>\pm</math> 0.007</b> | -                                  | -                                  | -           |

## 6. Related Work

The field of black-box visual search engine explainability is relatively new despite the ubiquity of search engines. To our knowledge (Dong et al.) is the first to present a generic visual search engine explanations. We also note the works of (Singh & Anand, 2019) and (Fernando et al., 2019) who marginally interpret a text search engine using LIME and DeepSHAP. However, these works do not apply their methods to images and do not lift these approaches to the joint domain. The optical-flow architecture FlowNet (Fischer et al., 2015) uses the correlation between convolutional feature maps to estimate the correspondence between two adjacent video frames as part of a larger optical flow architecture. Though similar to SAM, this approach was not interpreted in the context of search engine explanations. (Hou et al., 2019) also embeds a component similar to SAM within a deep classifier to improve few-shot performance. Other recent works have used learn co-attention within transformer architectures to help pool and share information across multiple domain types (Wei et al., 2020).

In the field of cooperative game theory, several seminal works provide a variety of ways to extend Shapley Values to more complex interactions. (Harsanyi, 1963) generalized the Shapely value by introducing a “dividend” that, when split and distributed among players, yields the Shapley Values. (Owen, 1972) introduce another way to extend Shapley values using a multi-linear extension of the game’s characteristic function. (Sundararajan et al., 2020) introduce the Shapley-Taylor index which they show is equivalent

to the Lagrangian remainder of Owen’s multi-linear extension. This work does not relate the Shapley-Taylor indices to Harsanyi dividends or explore interactions in the context search engine interpretability.

## 7. Conclusion

In this work we have proposed and evaluated new approaches to generate model-agnostic explanations for image similarity, search, and retrieval architectures. We characterize search engine interpretability methods as either “marginal” or “joint” interpretation methods depending on what kind of information they explain. We extended Class Activation Maps (CAMs), Additive Shapley Explanations (SHAP), and Locally Interpretable Model-Agnostic Explanations (LIME) to image retrieval and search and showed it was possible to extract much richer “joint” interpretations using extensions of these methods. These approaches enable black and grey-box model introspection and can help diagnose errors and understand the rationale behind a model’s similarity judgements. We also provide a new framework for deriving optimal credit assignments from Harsanyi Dividends. We show that this framework generalizes the Shapley-Taylor indices, and provide a Kernel for faster estimation of Shapley-Taylor indices. Finally, we show this game-theoretic formalism yields more faithful model interpretation strategies for several visual search engines.



## References

- Achanta, R., Shaji, A., Smith, K., Lucchi, A., Fua, P., and Süsstrunk, S. Slic superpixels. Technical report, 2010.
- Ahn, J., Cho, S., and Kwak, S. Weakly supervised learning of instance segmentation with inter-pixel relations. In *Proceedings of the IEEE Conference on Computer Vision and Pattern Recognition*, pp. 2209–2218, 2019.
- Bach, S., Binder, A., Montavon, G., Klauschen, F., Müller, K.-R., and Samek, W. On pixel-wise explanations for non-linear classifier decisions by layer-wise relevance propagation. *PLoS one*, 10(7):e0130140, 2015.
- Bengio, Y., Courville, A., and Vincent, P. Representation learning: A review and new perspectives. *IEEE transactions on pattern analysis and machine intelligence*, 35(8): 1798–1828, 2013.
- Bennett, J., Lanning, S., et al. The netflix prize. 2007.
- Bing. Beyond text queries: Searching with bing visual search, Jun 2017. URL <https://aka.ms/AAas7jg>.
- Dobrushin, R. L. Prescribing a system of random variables by conditional distributions. *Theory of Probability & Its Applications*, 15(3):458–486, 1970.
- Dong, B., Collins, R., and Hoogs, A. Explainability for content-based image retrieval.
- Einstein, A. The foundation of the general theory of relativity. the principle of relativity, 1923.
- Everingham, M., Van Gool, L., Williams, C. K. I., Winn, J., and Zisserman, A. The pascal visual object classes (voc) challenge. *International Journal of Computer Vision*, 88(2):303–338, June 2010.
- Fernando, Z. T., Singh, J., and Anand, A. A study on the interpretability of neural retrieval models using deepshap. In *Proceedings of the 42nd International ACM SIGIR Conference on Research and Development in Information Retrieval*, pp. 1005–1008, 2019.
- Fischer, P., Dosovitskiy, A., Ilg, E., Häusser, P., Hazırbaş, C., Golkov, V., Van der Smagt, P., Cremers, D., and Brox, T. Flownet: Learning optical flow with convolutional networks. *arXiv preprint arXiv:1504.06852*, 2015.
- Grabisch, M. et al. *Set functions, games and capacities in decision making*, volume 46. Springer, 2016.
- Hamilton, M., Fu, S., Freeman, W. T., and Lu, M. Conditional image retrieval. *arXiv preprint arXiv:2007.07177*, 2020.
- Harsanyi, J. C. A simplified bargaining model for the n-person cooperative game. *International Economic Review*, 4(2):194–220, 1963.
- Hastie, T. J. and Tibshirani, R. J. *Generalized additive models*, volume 43. CRC press, 1990.
- He, K., Zhang, X., Ren, S., and Sun, J. Deep residual learning for image recognition. In *Proceedings of the IEEE conference on computer vision and pattern recognition*, pp. 770–778, 2016.
- Hou, R., Chang, H., Ma, B., Shan, S., and Chen, X. Cross attention network for few-shot classification. *arXiv preprint arXiv:1910.07677*, 2019.
- Huang, G., Liu, Z., Van Der Maaten, L., and Weinberger, K. Q. Densely connected convolutional networks. In *Proceedings of the IEEE conference on computer vision and pattern recognition*, pp. 4700–4708, 2017.
- Kohavi, R., Wolpert, D. H., et al. Bias plus variance decomposition for zero-one loss functions. In *ICML*, volume 96, pp. 275–83, 1996.
- Koren, Y. The bellkor solution to the netflix grand prize. *Netflix prize documentation*, 81(2009):1–10, 2009.
- Lundberg, S. M. and Lee, S.-I. A unified approach to interpreting model predictions. In Guyon, I., Luxburg, U. V., Bengio, S., Wallach, H., Fergus, R., Vishwanathan, S., and Garnett, R. (eds.), *Advances in Neural Information Processing Systems 30*, pp. 4765–4774. Curran Associates, Inc., 2017.
- Nayak, P. Understanding searches better than ever before, Oct 2019. URL <https://blog.google/products/search/search-language-understanding-bert/>.
- Nelder, J. A. and Wedderburn, R. W. Generalized linear models. *Journal of the Royal Statistical Society: Series A (General)*, 135(3):370–384, 1972.
- Nori, H., Jenkins, S., Koch, P., and Caruana, R. Interpretml: A unified framework for machine learning interpretability. *arXiv preprint arXiv:1909.09223*, 2019.
- Owen, G. Multilinear extensions of games. *Management Science*, 18(5-part-2):64–79, 1972.
- Paszke, A., Gross, S., Massa, F., Lerer, A., Bradbury, J., Chanan, G., Killeen, T., Lin, Z., Gimelshein, N., Antiga, L., Desmaison, A., Kopf, A., Yang, E., DeVito, Z., Raison, M., Tejani, A., Chilamkurthy, S., Steiner, B., Fang, L., Bai, J., and Chintala, S. Pytorch: An imperative style, high-performance deep learning library. In Wallach, H., Larochelle, H., Beygelzimer, A., d'Alché-Buc,

- F., Fox, E., and Garnett, R. (eds.), *Advances in Neural Information Processing Systems 32*, pp. 8024–8035. Curran Associates, Inc., 2019.
- Rendle, S., Zhang, L., and Koren, Y. On the difficulty of evaluating baselines: A study on recommender systems. *arXiv preprint arXiv:1905.01395*, 2019.
- Ribeiro, M. T., Singh, S., and Guestrin, C. "why should I trust you?": Explaining the predictions of any classifier. In *Proceedings of the 22nd ACM SIGKDD International Conference on Knowledge Discovery and Data Mining, San Francisco, CA, USA, August 13-17, 2016*, pp. 1135–1144, 2016.
- Shapley, L. S. Notes on the n-person game—ii: The value of an n-person game. 1951.
- Shrikumar, A., Greenside, P., and Kundaje, A. Learning important features through propagating activation differences, 2017.
- Simonyan, K. and Zisserman, A. Very deep convolutional networks for large-scale image recognition. *arXiv preprint arXiv:1409.1556*, 2014.
- Singh, J. and Anand, A. Exs: Explainable search using local model agnostic interpretability. In *Proceedings of the Twelfth ACM International Conference on Web Search and Data Mining*, pp. 770–773, 2019.
- Su, X. and Khoshgoftaar, T. M. A survey of collaborative filtering techniques. *Advances in artificial intelligence*, 2009, 2009.
- Sundararajan, M., Taly, A., and Yan, Q. Axiomatic attribution for deep networks. In *International Conference on Machine Learning*, pp. 3319–3328. PMLR, 2017.
- Sundararajan, M., Dhamdhere, K., and Agarwal, A. The shapley taylor interaction index. In *International Conference on Machine Learning*, pp. 9259–9268. PMLR, 2020.
- Wang, Y., Zhang, J., Kan, M., Shan, S., and Chen, X. Self-supervised equivariant attention mechanism for weakly supervised semantic segmentation. In *Proceedings of the IEEE/CVF Conference on Computer Vision and Pattern Recognition*, pp. 12275–12284, 2020.
- Wei, X., Zhang, T., Li, Y., Zhang, Y., and Wu, F. Multi-modality cross attention network for image and sentence matching. In *Proceedings of the IEEE/CVF Conference on Computer Vision and Pattern Recognition*, pp. 10941–10950, 2020.
- Young, H. P. Monotonic solutions of cooperative games. *International Journal of Game Theory*, 14(2):65–72, 1985.
- Zhou, B., Khosla, A., A., L., Oliva, A., and Torralba, A. Learning Deep Features for Discriminative Localization. *CVPR*, 2016.

## Appendix

### A. Generalizing SBSM to Joint Search Engine Interpretability

Before generalizing SBSM (Dong et al.) to joint interpretability we will review the original implementation for marginal interpretability. SBSM uses a sliding square mask and multiple evaluations of the search engine in order to determine which regions of the image are important for similarity. More formally, let  $q$ , and  $r$  represent the pixels of the query image and retrieved image. Let  $M_{ij}^s(q)$  represent the result of replacing a square of pixels of size  $s \times s$  centered at pixel  $(i, j)$  with a “background value” which in our case is black. SBSM “slides” this mask across the query image and compares the similarity between the masked query and retrieved image. These masked similarity values are compared to the baseline similarity value and stored in a weight matrix,  $w$ :

$$w_{ij} = \min [d(M_{ij}^s(q), r) - d(q, r), 0] \quad (11)$$

Intuitively speaking, the weights  $w_{ij}$  represent the impact of masking a square centered at  $(i, j)$ . For areas that are critical to the similarity, this will result in  $w_{ij} > 0$ . Finally an attention mask on the query image is formed by a weighted average of the masks used to censor the images. For square masks, this can be achieved efficiently using a deconvolution with a kernel of ones of size  $s \times s$  on the weight matrix  $w$ . We also note that instead of evaluating the (expensive) distance computation  $d$  for every pixel  $(i, j)$ , one can also sample pixels to censor. We use this approach in our joint generalization.

To generalize SBSM we use a pair of masks, one for the query image and one for the retrieved image respectively. We sample mask locations and calculate weights designed to capture the intuition that censoring corresponding areas cause similarity to increase as oppose to decrease. More specifically we use the following weighting scheme:

$$w_{ij}^{hw} = \min [d(q, r) - d(M_{ij}^s(q), M_{hq}^s(r)), 0] \quad (12)$$

Because evaluating the similarity function for every  $(i, j, h, w)$  combination is prohibitively expensive, we instead sample masked images for our computation. To project attention from a query pixel, we query for all masks that overlap with the selected query pixel, and then average their corresponding retrieved masks according to the weights calculated in Equation 12.

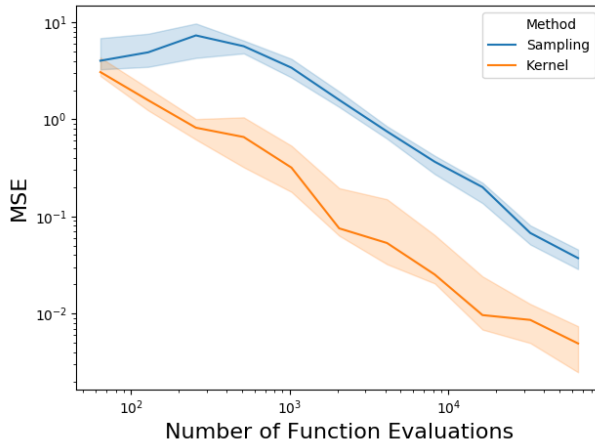


Figure 7. Convergence of Shapley-Taylor index estimation schemes with respect to the Mean Squared Error (MSE). Our proposed kernel estimation strategy converges with significantly fewer function evaluations.

### B. Accelerated Convergence of Kernel-Based Shapley-Taylor Estimation

Though the Harsanyi Dividends and Shapley-Taylor indices provide a robust way to allocate credit, they are difficult to compute. The authors of the Shapley-Taylor indices provide a sampling-based approximation, but this approach requires estimating each interaction term with a separate sampling procedure. To make this approach more tractable for large scale datasets we draw a parallel the unification of LIME with Shapley Values through a specific weighting kernel. We find that unlike Shapley-Taylor sampling procedures, this requires significantly fewer function evaluations to converge to the true Shapley-Taylor indices.

We quantify this speedup by measuring convergence to the brute-force calculated Shapley-Taylor indices for random 8 dimensional Boolean functions formed by randomly assigning each subset a random integer in  $[0, 10]$ . Figure 7 shows that Kernel based approximation has a much better sample complexity than Shapley-Taylor sampling approaches.